The Power of Two: ARGININE 51 AND ARGININE 239* FROM A NEIGHBORING SUBUNIT ARE ESSENTIAL FOR CATALYSIS IN α-AMINO-β-CARBOXYMUCONATE-?-SEMIALDEHYDE DECARBOXYLASE

Lu Huo, Ian Davis, Lirong Chen and Aimin Liu

Access the most updated version of this article at doi: 10.1074/jbc.M113.496869

Find articles, minireviews, Reflections and Classics on similar topics on the JBC Affinity Sites.

Alerts:
- When this article is cited
- When a correction for this article is posted

Click here to choose from all of JBC's e-mail alerts

This article cites 45 references, 9 of which can be accessed free at
http://www.jbc.org/content/288/43/30862.full.html#ref-list-1

The Power of Two

ARGININE 51 AND ARGININE 239* FROM A NEIGHBORING SUBUNIT ARE ESSENTIAL FOR CATALYSIS IN α-AMINO-β-CARBOXYMUCONATE-ε-SEMIALDEHYDE DECARBOXYLASE*

Lu Huo[1]**, Ian Davis, Lirong Chen, and Aimin Liu**[2]

From the Department of Chemistry and Center for Diagnostics and Therapeutics, Georgia State University, Atlanta, Georgia 30303

Background: α-Amino-β-carboxymuconate-ε-semialdehyde decarboxylase is a key enzyme that controls quinolinic acid levels.
Results: Two arginines, including one from a neighboring subunit, are required for substrate binding.
Conclusion: Dimerization and two arginine residues are required for activity.
Significance: This study provides the first structurally proven example of a functionally active heterodimer hybrid resulting from a simple mixing of two inactive homodimer mutants.

Although the crystal structure of α-amino-β-carboxymuconate-ε-semialdehyde decarboxylase from *Pseudomonas fluorescens* was solved as a dimer, this enzyme is a mixture of monomer, dimer, and higher order structures in solution. In this work, we found that the dimeric state, not the monomeric state, is the functionally active form. Two conserved arginine residues are present in the active site: Arg-51 and an intruding Arg-239* from the neighboring subunit. In this study, they were each mutated to alanine and lysine, and all four mutants were catalytically inactive. The mutants were also incapable of accommodating pyridine-2,6-dicarboxylic acid, a competitive inhibitor of the native enzyme, suggesting that the two Arg residues are involved in substrate binding. It was also observed that the decarboxylase activity was partially recovered in a heterodimer hybridization experiment when inactive R51(A/K) and R239(A/K) mutants were mixed together. Of the 20 crystal structures obtained from mixing inactive R51A and R239A homodimers that diffracted to a resolution lower than 3.00 Å, two structures are clearly R51A/R239A heterodimers and belong to the C2 space group. They were refined to 1.80 and 2.00 Å resolutions, respectively. Four of the remaining crystals are apparently single mutants and belong to the P4$_2$2$_1$2 space group. In the heterodimer structures, one active site is shown to contain dual mutation of Ala-51 and Ala-239*, whereas the other contains the native Arg-51 and Arg-239* residues, identical to the wild-type structure. Thus, these observations provide the foundation for a molecular mechanism by which the oligomerization state of α-amino-β-carboxymuconate-ε-semialdehyde decarboxylase could regulate the enzyme activity.

Arginine residues perform diverse functions in proteins because of their charge distribution, their capability of forming multiple hydrogen bonds, and their long flexible side chains. One popular function is the formation of salt bridges in which the positively charged guanidine head pairs with a negatively charged carboxylate group (1, 2). In enzymes, arginine residues are often proposed to participate in recognizing, binding, and maintaining the orientation of substrates and reaction intermediates (3–5). Arginine is also involved in RNA recognition because its guanidium group is able to form five hydrogen bonds with RNA acceptor groups (6). Although not widespread, arginine residues have also recently been proposed to act as a general base in several enzymes (7–9).

Two arginine residues in α-amino-β-carboxymuconate-ε-semialdehyde decarboxylase (ACMSD)[3] caught our attention because they appear to be in an optimal position to bind the substrate α-amino-β-carboxymuconate-ε-semialdehyde (ACMS) by interacting with its two carboxyl groups. ACMSD is a metal-dependent enzyme in the amidohydrolase superfamily (10, 11), and its substrate, ACMS, is an unstable tryptophan catabolic intermediate in the kynurenine pathway (11–13). The conversion of ACMS to α-amino muconate-ε-semialdehyde is catalyzed by ACMSD; however, ACMS spontaneously forms quinolinic acid (QA) in a nonenzymatic dehydration process in the absence of ACMSD (14, 15) (Scheme 1). Thus, ACMSD is a key enzyme that determines the QA levels. QA is maintained only at the basal level for the *de novo* synthesis of a small fraction of NAD$^+$ in mammals. Reduced activity of ACMSD leads to accumulation of QA in body fluids, a condition that is known to be related to several neurodegenerative diseases including Alzheimer disease (16), Huntington disease (17), stroke (12), and epilepsy (12, 13, 18). However, the instability of ACMS and the compounds with similar structures makes studying the mechanism of ACMSD substrate binding technically challenging.

The first crystal structure of ACMSD was solved as a homodimer from *Pseudomonas fluorescens* (19). Two strictly
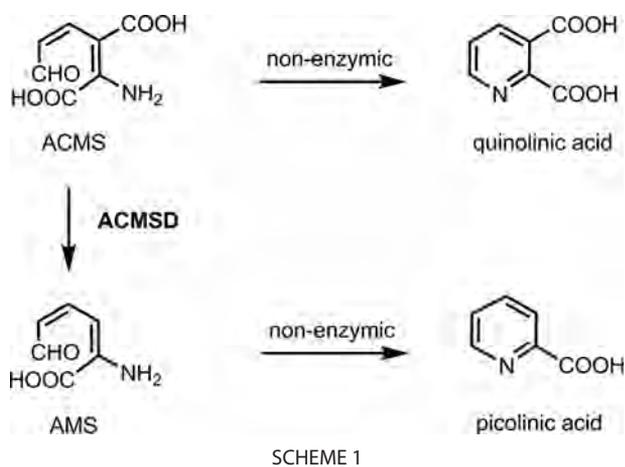
---

[3] The abbreviations used are: ACMS, α-amino-β-carboxymuconate-ε-semialdehyde; ACMSD, ACMS decarboxylase; PDC, pyridine-2,6-dicarboxylic acid; QA, quinolinic acid.
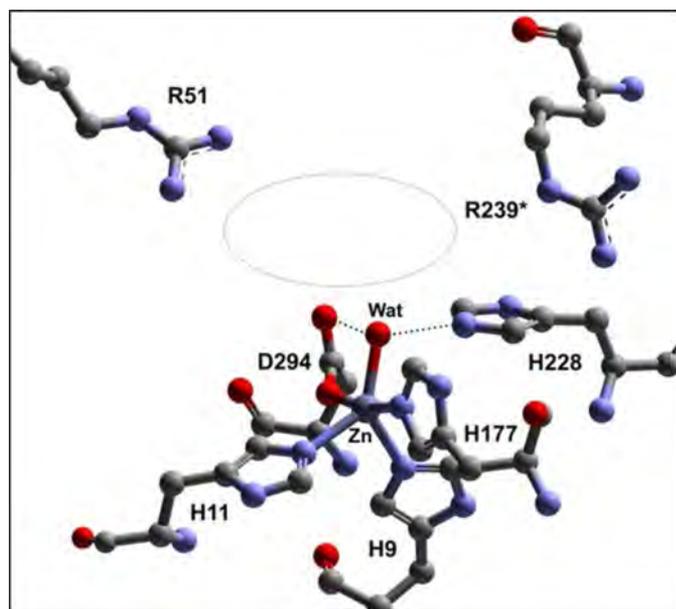
SCHEME 1

FIGURE 1. **The active site metal center of *P. fluorescens* ACMSD (Protein Data Bank code 2HBV) and the putative substrate-binding pocket (illustrated with an ellipse).** His-228 is a previously identified acid-base catalyst. Arg-51 lies in the putative substrate-binding pocket, and Arg-239* is an intruding residue from the neighboring subunit.

conserved arginine residues are present at the active site: Arg-51 and Arg-239* (Fig. 1). Arg-51 is located in the mobile insertion domain, which is proposed to undergo conformational changes upon substrate binding because of its unique position and high flexibility (19). Arg-239* is an intruding residue that is inserted from the sixth α-helix of the other subunit, and it is labeled with a * hereafter to distinguish its origin from the chain of a neighboring subunit. Because of its high flexibility, this residue is shown to be present in alternative conformations in chain B of the crystal structure.

The second ACMSD crystal structure is the human enzyme in complex with 1,3-dihydroxyacetone-phosphate. This inactive complex was assigned as a monomer by Rizzi and co-workers (20). The equivalent residue of Arg-51 is shown in the active site, but the counterpart of Arg-239 is far removed from the catalytic center. The same group previously reported that functional human ACMSD is a monomer because gel filtration chromatography showed the as-isolated enzyme with a molec-

ular mass of ~50 kDa (21), which is between monomer (38 kDa) and dimer (76 kDa) mass. In fact, it is still unclear whether the catalytically active form of human ACMSD in solution is a monomeric or dimeric enzyme at the present time. All of the *P. fluorescens* ACMSD structures determined thus far, including wild type and mutants charged with different transition metals, are dimeric (19, 22). If the monomeric form is catalytically active, then only one conserved arginine residue, Arg-51, is present in the active site of the enzyme in both human ACMSD and *P. fluorescens* ACMSD structures. Arg-239 of the same subunit is not located near the enzyme active site in the monomeric state and would therefore be less likely to be an essential component of catalysis. Thus, point mutation at residue 239 provides a sensible means for probing the effects of protein oligomerization on the catalytic activity.

The present work represents the first attempt to investigate the molecular mechanism by which the oligomerization state of ACMSD could determine the enzyme activity. The quaternary state required for catalytic activity is reported, and the catalytic roles of the two conserved arginine residues, Arg-51 and the intruding Arg-239* from the neighboring subunit, are proposed. Interestingly, we found that the inactive Arg-51 and Arg-239 mutants could form a crystallographically accessible, catalytically active heterodimer through protein hybridization.

EXPERIMENTAL PROCEDURES

Site-directed Mutagenesis—R51A, R51K, R239A, and R239K single mutation mutants were constructed by using the PCR overlap extension mutagenesis technique (23) described previously (10) and by using the plasmid containing ACMSD from *P. fluorescens* as a template (11). The mutants were verified by DNA sequencing to ensure that base changes were introduced correctly and that no random changes had occurred. After sequencing, the positive clone was used for protein expression in *Escherichia coli* BL21(DE3).

Protein Preparation, SDS-PAGE, and Size Exclusion Chromatography—Expression and purification of ACMSD proteins followed the protocol established previously (10, 11, 22, 24) with a few minor changes. Rather than using pH 8.0 buffer during affinity chromatography purification, buffer at pH 7.4 was used to increase protein stability of the mutants. Metal-free apoenzyme was obtained by treating purified protein with 5 mM EDTA for 12 h followed by running a G50 desalting column. Zn(II)- and Co(II)-containing ACMSD were reconstituted as previously described (11). Purified protein samples were mixed with SDS loading buffer and heated for 10 min or with no heating prior to loading to 10% SDS-PAGE. ACMSD was loaded onto a Superdex 75 column pre-equilibrated with buffer containing 25 mM HEPES (pH 7.0) and 5% glycerol (v/v). Protein was eluted with the same buffer.

Enzyme Activity Assay—The substrate ACMS was generated enzymatically by catalyzing the dioxygenation of 3-hydroxyanthranilic acid in oxygen saturated buffer with ferrous 3-hydroxyanthranilate 3,4-dioxygenase containing no free transient metal ion as reported previously (10, 11, 22). Briefly, the ACMSD enzyme assay mixture contained 5–120 μM ACMS and an appropriate amount of ACMSD protein in 25 mM HEPES buffer with 5% glycerol, pH 7.0. Specific activities of

Dimerization Is Required for Activity in ACMSD

ACMSD proteins were measured in triplicate at room temperature on an Agilent 8453 spectrophotometer by monitoring the decrease of ACMS absorbance at 360 nm using a molar extinction coefficient of 47,500 M^{-1} cm^{-1} (25) when the substrate concentration was equal to or lower than 20 μM, or at 320 nm using a molar extinction coefficient of 9600 M^{-1} cm^{-1} when the substrate concentration was higher than 20 μM (10).

Derivation of Equations for Analysis of the Correlation of Monomer/Dimer Ratio and Catalytic Activity—To show that dimerization is required for catalytic activity, a series of activity assays were performed in which the stock concentration of ACMSD is varied while keeping the final assay concentration constant. If the rate of dissociation of the ACMSD dimers is sufficiently slow on the time scale of the assay, then the measured activity should conform to Equation 1, where k_{obs} is the observed decarboxylation rate, k_{max} is the maximum rate, and %D is the mole ratio of dimer present in the assay.

$$k_{obs} = k_{max} \cdot \%D \qquad \text{(Eq. 1)}$$

To solve for the percent dimer, mass balance was invoked to define M_0 as the total protomer concentration, M as the monomer concentration, and D as the dimer concentration.

$$\text{if } M_0 = M + 2D, \text{ then } M = M_0 - 2D \qquad \text{(Eq. 2)}$$

The dimer percentage can then be written in terms of dimer concentration and total protomer concentration (a quantity that is known in an activity assay) alone.

$$\%Dimer = \frac{2D}{M_0} \qquad \text{(Eq. 3)}$$

The association constant for this equilibrium can then be written in terms of dimer concentration and total protomer concentration by substitution of Equation 2, as seen in Equation 4.

$$K_a = \frac{D}{(M_0 - 2D)^2} \qquad \text{(Eq. 4)}$$

Distribution and collection of like terms then gives Equation 5, and Equation 5 can be multiplied by M_0^{-2} to give Equation 6.

$$4K_a D^2 - (4K_a M_0 + 1)D - K_a M_0^2 = 0 \qquad \text{(Eq. 5)}$$

$$K_a \frac{4D^2}{M_0^2} - \left(2K_a + \frac{1}{2M_0}\right)\frac{2D}{M_0} - K_a = 0 \qquad \text{(Eq. 6)}$$

The quadratic equation can now be invoked on Equation 6 to solve directly for the dimer percentage and is shown in Equation 7. Multiplying the right side of Equation 7 by a disguised 1, ($2M_0/2M_0$), the expression for the dimer percentage can be simplified to Equation 8.

$$\frac{2D}{M_0} = \frac{\left(2K_a + \frac{1}{2M_0}\right) \pm \sqrt{\left(2K_a + \frac{1}{2M_0}\right)^2 - 4K_a^2}}{2K_a}$$

$$\text{(Eq. 7)}$$

$$\%D = 1 + \frac{1 \pm \sqrt{8K_a M_0 + 1}}{4K_a M_0} \qquad \text{(Eq. 8)}$$

Substitution of Equation 8 back into Equation 1 gives k_{obs} as a function of k_{max}, K_a, and M_0 (*i.e.*, Equation 9). Nonlinear least squares fitting can then be used to obtain both K_a and k_{max} (though both positive and negative square roots should be considered, only the negative roots gave convergent fits of the measured data).

$$k_{obs} = k_{max} \cdot \left(1 + \frac{1 - \sqrt{8K_a M_0 + 1}}{4K_a M_0}\right) \qquad \text{(Eq. 9)}$$

Protein Hybridization—Arg-51 and Arg-239 mutants were mixed in a 1:1 ratio in 25 mM HEPES buffer, pH 7.0, containing 5% glycerol. The final protein concentration for each mutant was 12 μM. Specific activity of the mixtures was examined frequently after mixing by a spectrophotometric assay on an Agilent 8453 diode array spectrophotometer as described above.

Identification of a Competitive Inhibitor—Pyridine-2,6-dicarboxylic acid (PDC) inhibition pattern and constant were determined by measuring k_{cat} and K_m in the presence of varying inhibitor concentrations (0, 20, 40, and 80 μM). Apparent K_m values for each inhibitor concentration were plotted as a function of inhibitor concentration, and inhibition is expressed as K_i values in micromolar (K_i = intercept/slope).

Analysis of PDC Inhibitor Interaction with the Arginine Mutants—PDC in HEPES buffer displays UV absorbance at 270 nm with extinction coefficient of 4,100 M^{-1} cm^{-1}. ACMSD proteins (1.5 ml, 40 μM in each sample type), including wild type, R51A, R239A, H228G, and premixed R51A and R239A for 48 h, were incubated with one equivalent of PDC for 5 min in separate experiments, followed by filtration in an Amicon ultra centrifugal filter tube with cellulose membrane of 10,000-dalton cutoff. PDC (40 μM) with no protein was used in the control experiment. Samples were centrifuged in 3,000 $\times$ g for 8 min. The flow-through solution containing unbound DPA was quantified by an Agilent 8453 spectrophotometer.

X-ray Data Collection and Crystallographic Refinement—Zinc-reconstituted mutant proteins were used for crystallization. All single crystals were obtained following the crystallization conditions described in the previous studies (19, 22). For the heterodimer crystal, R51A and R239A were mixed for more than 48 h at 4 °C before being used for crystallization by hanging drop vapor diffusion in VDX plates (Hampton Research). Mother liquid containing 20% ethylene glycol was used for crystal mounting. X-ray diffraction data were collected at SER-CAT Beamline 22-ID/BM of the Advanced Photon Source (Argonne National Laboratory, Argonne, IL). Data were processed with HKL-2000 (26). Structure solutions were obtained by molecular replacement with MolRep (27) from the CCP4 suite (28) with wild-type ACMSD (Protein Data Bank code 2HBV) as the search model (19). Refinement was carried out using PHENIX software (29), and the model building was carried out in COOT (30). Ala-51 and Ala-239 were modeled based on the $2F_o - F_c$ and $F_o - F_c$ electron density maps. Refinement was assessed as complete when the $F_o - F_c$ electron density contained only noise.
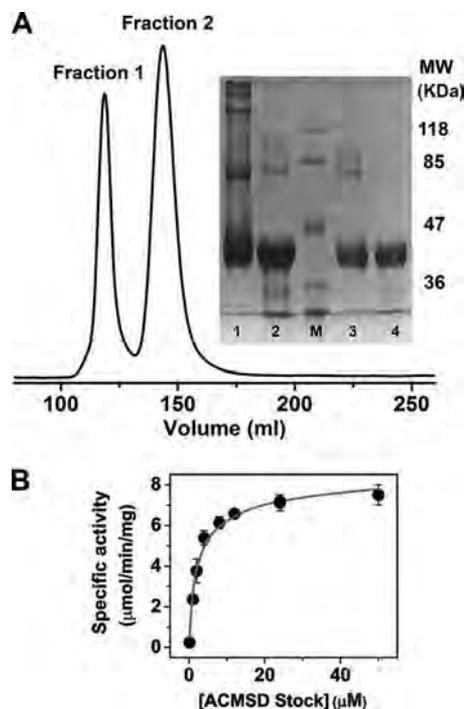
FIGURE 2. *A*, the UV absorbance at 280 nm of ACMSD as a function of the elution volume from size exclusion chromatography column: Superdex 75. Fraction 1 corresponds to molecular mass (*MW*) larger than 100 kDa, and fraction 2 has a molecular mass of ~51 kDa. The *inset* is an SDS-PAGE. *Lane 1*, as-isolated ACMSD with no heating; *lane 2*, as-isolated ACMSD heated for 10 min; *lane M*, molecular marker; *lane 3*, fraction 2 with no heating; *lane 4*, fraction 2 heated for 10 min. *B*, the specific activity of ACMSD as a function of different enzyme stock concentration. The final reaction concentration of the enzyme was kept constant at 0.1 μM, and the data were fit to Equation 9.

RESULTS

ACMSD Does Not Exist as a Single Species in Solution—As shown in Fig. 2*A*, ACMSD presents several bands by SDS-PAGE that correspond to monomer, dimer, and higher order oligomerization states if the sample is not heated before loading onto the gel (Fig. 2*A*, *lane 1*). However, if the sample is heated before loading, the bands corresponding to the higher order states and most of the dimer are not observed (Fig. 2*A*, *lane 2*). The size exclusion chromatography profile, on the other hand, presents two major peaks. The molecular mass of the protein eluted in the first peak is larger than 100 kDa, and the second peak exhibits a molecular mass of ~51 kDa. The molecular mass of a *P. fluorescens* ACMSD monomer, however, is 38 kDa. Also, there is no difference in the specific activity of the two fractions as they elute from the column. The second peak shows two major bands corresponding to ACMSD monomer and dimer molecular masses on SDS-PAGE when not heated before loading (Fig. 2*A*, *lane 3*). The band that arises from the dimer is not observed upon heating of the sample before loading (Fig. 2*A*, *lane 4*). Hence, we assign the second peak as a combination of ACMSD monomer and dimer and the first peak as a mixture of higher order complexes that are not able to be resolved further.

To estimate the dimer dissociation constant, ACMSD was prepared in stock concentrations ranging from 0.1 to 50 μM (protomer concentration) and allowed to equilibrate at 4 °C for 24 h. Specific activity of the different stock concentrations was determined by keeping the final enzyme and substrate concentrations constant. The specific activity increased with increasing stock concentration. Decarboxylation rates as a function of enzyme stock concentration were plotted in Fig. 2*B*, and the data were fit to Equation 9, which represents the equilibrium of ACMSD between inactive monomer and active dimer forms as described under "Experimental Procedures." Fitting of the data to Equation 9 gives a K_a of 3.3×10^6 M^{-1} and a maximum specific activity of 9.4 μmol·min^{-1}·mg^{-1}.

Mutational Analysis and Catalytic Activity Rescue through Protein Hybridization—Arg-51 and Arg-239 were each mutated to alanine and lysine. All of the four mutants were found to be completely inactive with either zinc or cobalt as the cofactor, the two metals that were previously found to be optimal for catalytic activity in the wild-type enzyme. Chemical rescue performed on R51A and R239A by guanidine derivatives was unsuccessful in restoring enzymatic activity. However, when the two mutants, R51A and R239A, were mixed together, enzyme activity was slowly restored (Fig. 3*A*). The reaction rates were determined at several time points after mixing. Samples incubated for 1, 7, and 24 h on ice were analyzed by following decay of the substrate ACMS at 360 nm for 1 min. Reaction with no enzyme and the two inactive arginine mutants were used as negative controls. The rate of activity rescue was temperature-dependent, and the rate of recovery was faster when the mixing reaction was carried out at room temperature rather than on ice. The specific activity was calculated and plotted as a function of incubation time as shown in Fig. 3*B* and fit to a single exponential association, Equation 10, where *A* is the measured specific activity, $A_{\max}$ is the maximum activity, *k* is the associative rate constant, and *t* is time in minutes. According to the fitting, the maximum rate is 152 ± 5 nmol·min^{-1}·mg^{-1}, and the rate constant is $7.2 \pm 0.5 \times 10^{-3}$ min^{-1}. We also determined kinetic parameters for the mixed zinc-reconstituted mutants after 48 h of equilibration on ice. Fig. 3*C* shows the Michaelis-Menten plot. The K_m, 9.3 ± 1 μM, of the mixed mutants is similar to that of the wild-type Zn-ACMSD, 9.6 μM. The k_{cat}, 0.15 ± 0.01 s^{-1}, of the mixed mutants, on the other hand, is dramatically decreased compared with the 6.5 s^{-1} of the WT Zn-ACMSD (19).

$$A = A_{\max} \cdot (1 - e^{-kt}) \qquad \text{(Eq. 10)}$$

Structural Determination of R51A, R239A, and the Hybridized Mixtures of the Two Mutants—All crystals of R51A and R239A ACMSD belong to the P4$_2$2$_1$2 space group. They diffracted poorly and only at relatively low resolutions. The best structures obtained were 2.50 Å resolution for R51A (Protein Data Bank code 4IFO) and 2.40 Å for R239A (Protein Data Bank code 4IFR). Interestingly, crystals from the mixture of these two mutants were crystallized in both the P4$_2$2$_1$2 and C2 space groups.

A total of 20 data sets were collected from individual single crystals obtained from crystallization trays with equal molar ratio mixing of R51A and R239A mutant proteins. Among the 20 crystal structures that we have solved, three of them are R239A homodimer, and one of them is an R51A homodimer. All of these four structures are determined in the P4$_2$2$_1$2 space group. Two single crystals were found to belong to the C2 space

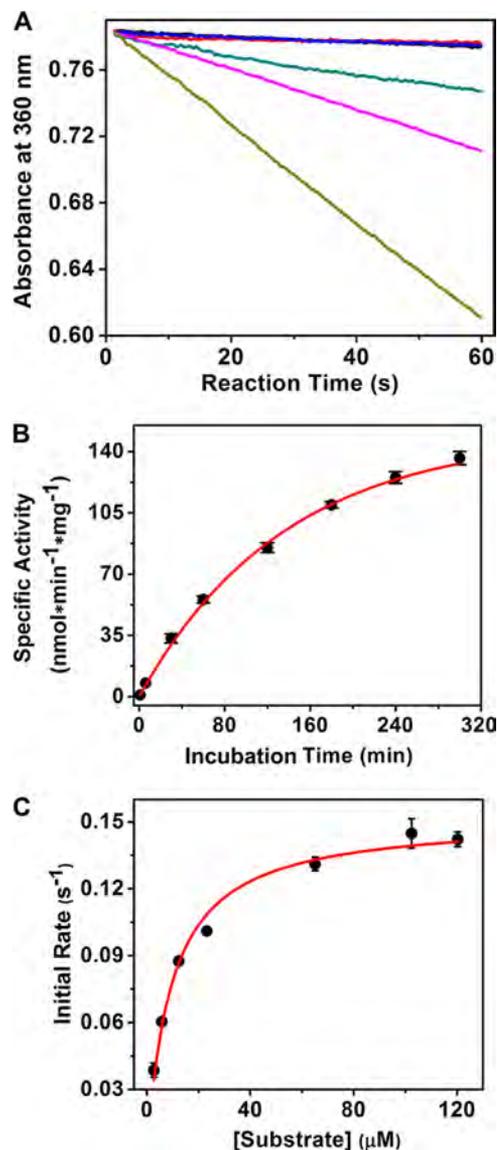## Dimerization Is Required for Activity in ACMSD

FIGURE 3. *A*, catalytic activity rescue of mixed R51A and R239A mutants. Decay of the substrate, ACMS, in the first minute was monitored by UV-visible spectroscopy at 360 nm. Autodecay of substrate (*black trace*), in the presence of R51A (*red trace*), and in the presence of R239A (*blue trace*) are three overlapping lines. R51A and R239A were premixed on ice for 1 h (*green trace*), 7 h (*pink trace*), and 24 h (*tan trace*), respectively. *B*, the rescued activity increased as a function of incubation time of the two mutants. The data were fit to Equation 10. The incubation and kinetic reaction are done at room temperature. *C*, Michaelis-Menten kinetics of the 1:1 mixed R51A and R239A after 48 h of equilibration.

group, and they were refined to 1.8 Å (Protein Data Bank entry 4IG2) and 2.0 Å (Protein Data Bank entry 4IFK) resolutions, respectively. The structures determined from these two crystals clearly differ from R51A or R239A, and they fit the proposed heterodimer as illustrated in Fig. 4. Fourteen of the data sets in the $P4_22_12$ space group cannot be assigned to any homodimer or heterodimer because of incomplete electron density that might be caused by the flexibility of the arginine side chain or low arginine occupancy. The data collection and refinement statistics for both the homodimer single mutants and the heterodimers are listed in Table 1.

Both DNA sequencing and electron density map of the mutant crystal structures demonstrate the successful substitu-

tion of arginine residues with alanine in both R51A and R239A variants (Fig. 5*A*, *top* and *middle panels*). The alignment of R51A (Protein Data Bank entry 4IFO) and R239A (Protein Data Bank entry 4IFR) structures with the wild-type structure (Protein Data Bank entry 2HBV) are shown in Fig. 5*B* (*top* and *middle panels*), respectively. Both mutants exhibit homodimeric quaternary structures as previously seen in wild-type ACMSD. Secondary structure changes caused by mutation (colored in *blue* and *cyan*) can be observed in both subunits of the two structures, and they are mainly observed in the loop regions. No significant structural deviations, however, were observed for the folding of the overall TIM barrel scaffold, indicating that the impact caused by mutation is limited to specific flexible regions. We further analyzed the dimerization interface using the ACMSD wild-type and mutant structures at an online server: Protein Data Bank Europe Protein Interfaces, Surfaces and Assemblies (PDBePISA) (31). The results indicate that the interface contains a total of 13 H-bonds and 13 salt bridges. Nevertheless, these analyses would not be sufficient to draw a definitive conclusion if there were no intruding residue Arg-239 catalytically important, which allowed us to generate an active heterodimer from mixing the two inactive dimers. In the wild-type structure, Arg-239 contributes two H-bonds by interacting with the main chain molecules of the neighboring monomers to help to stabilize the dimer. In the R239A structure, the dimerization is not interrupted because these two hydrogen bonds are substituted by the following two new H-bonding interactions: Glu-252 of chain A interacts with Lys-189 of chain B and Arg-247 of chain A interacts with Met-191 of chain B.

Fig. 5*B* (*bottom panel*) shows the superimposition of the heterodimer structure (Protein Data Bank code 4IFK) and the wild-type Zn-ACMSD structure (Protein Data Bank code 2HBV). The structural deviations of the mutant relative to the wild type are highlighted in *red*. The comparison clearly shows that major changes can only be observed in chain B. This observation is expected because in subunit A of the heterodimer, Arg-51 and Arg-239* are both in place with electron density similar to that in the wild-type structure (Fig. 5*A*, *bottom panel*). The electron density for the side chains of both arginine residues in subunit B is missing, indicating that both residues 51 and 239* are alanines (Fig. 5*A*, *bottom panel*). Hence, subunit A represents a complete native-like ACMSD subunit, but subunit B is a "double mutant" containing two alanine residues. It is noted in the structure of the native enzyme that Arg-239* adopts two conformations because of its high flexibility (19). Likewise, this residue in subunit A has alternative conformations that are only partially covered by the electron density map.

Arg-51 and Arg-239 Are Essential for Substrate Binding—Based on the current and previous studies, we propose that the two arginines are critical for proper substrate binding at the enzyme active site and for preventing its autocyclization to QA. Because the substrate, ACMS, is unstable and all arginine mutants are catalytically inactive, studying the postulated role of the two arginines in substrate binding is challenging. Therefore, an efficient competitive inhibitor needs to be found. Unfortunately, the inhibitors reported from previous *in vivo* studies, phthalate esters for instance (32, 33), were not effective
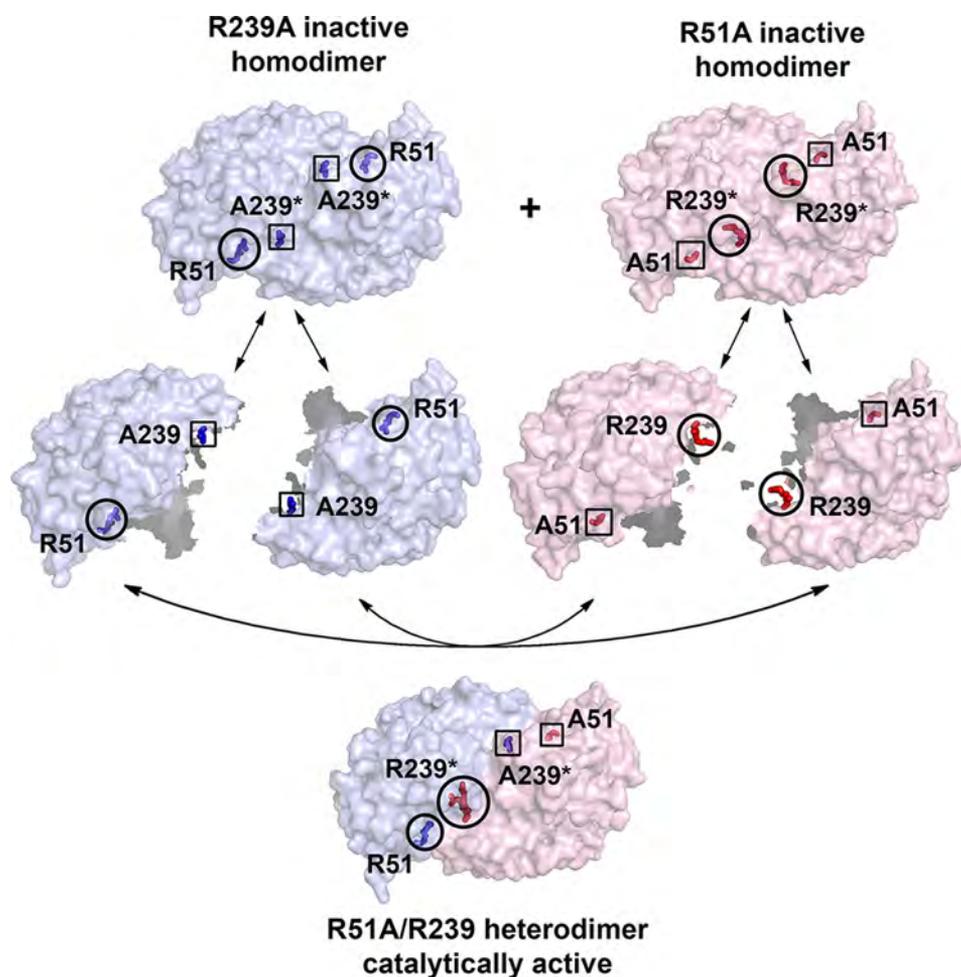
FIGURE 4. **Molecular mechanism for catalytic activity rescue through protein hybridization of the two completely inactive mutants, R51A and R239A.** *Blue* represents R239A, whereas *pink* represents R51A. *Circles* indicate native residues, and *rectangles* indicate mutated residues.

on the pure enzyme in our experiments. Acyclic ACMS analog compounds tend to be unstable in solution; however, PDC, a cyclic compound, is structurally similar to ACMS (Fig. 6A). Both compounds contain conjugate repeating single-bond double-bond structures and two carboxylate groups. The difference is that PDC is a stable compound because of its cyclic, aromatic structure, whereas ACMS tends to dehydratively autocyclize. Fig. 6B shows that PDC behaves kinetically as a competitive inhibitor for the ACMS decarboxylation. The K_i value was determined to be 22.7 $\pm$ 1.8 μM. This allows for use of PDC as an analog of ACMS to study substrate binding.

The catalytic activity-based kinetic approach, unfortunately, cannot be employed to assess the binding of substrate or substrate analog compounds to the inactive mutant proteins. We took advantage of the fact that PDC has an electronic absorption band at 270 nm ($\epsilon_{270\,nm}$ = 4100 M^{-1} cm^{-1}, determined in 25 mM HEPES buffer, pH 7.0) and designed an experiment to test the binding of PDC to the wild-type and mutant proteins of ACMSD utilizing separation by centrifuge filters. The threshold for membranes in centrifuge filters with a 10,000-Da cutoff is smaller than ACMSD but much larger than PDC. If the PDC is bound to ACMSD, it will not be able to pass the filter membrane, whereas unbound PDC molecules can pass freely. The amount of PDC in the flow-through was quantitated by UV

absorbance. Wild-type ACMSD was employed as a positive control, whereas the same buffer containing no protein was used as one negative control. A previously well characterized mutant H228G (22) was also employed as a secondary positive control. His-228 is a strictly conserved residue sitting in the interior side of the metal center that has been previously shown to function as a general base to deprotonate the water ligand during catalysis and that is not related with substrate binding. The properties and crystal structure of H228G have been reported previously (22). Fig. 6C shows that WT and H228G ACMSD proteins exhibit similar binding ability toward PDC. In contrast, R51A and R239A are unable to effectively bind PDC as exhibited by the similar absorbance of their flow-throughs to the negative control. This experiment suggests that the two arginine residues play an important role in binding of the substrate analog, which implies that they play a role in substrate binding in the native enzyme.

DISCUSSION

It is often a challenging task to determine whether or not an experimentally determined structure represents the biologically relevant assembly. It is also often difficult to pin down the role of a critical residue in catalysis when its mutants are completely inactive. An additional complexity in the present case is

Dimerization Is Required for Activity in ACMSD

TABLE 1

X-ray crystallography data collection and refinement statistics

Data collection	R51A-R239A Heterodimer 1	R51A-R239A Heterodimer 2	R51A Homodimer	R239A Homodimer
Detector type	MAR225 CCD	MAR300 CCD	MAR300 CCD	MAR300 CCD
Source	APS, Sector 22-BM	APS, Sector 22-ID	APS, Sector 22-ID	APS, Sector 22-ID
Space group	C2	C2	$P4_22_12$	$P4_22_12$
Unit cell lengths (Å)	$a = 153.10$, $b = 48.52$, $c = 109.83$	$a = 153.85$, $b = 49.06$, $c = 110.55$	$a = b = 91.21$, $c = 170.47$	$a = b = 91.16$, $c = 167.99$
Unit cell angles (°)	$\alpha = \gamma = 90$, $\beta = 126.80$	$\alpha = \gamma = 90$, $\beta = 127.10$	$\alpha = \beta = \gamma = 90$	$\alpha = \beta = \gamma = 90$
Wavelength (Å)	1.00	0.80	0.80	0.80
Temperature (K)	100	100	100	100
Resolution (Å)[a]	35.00–1.80 (1.86–1.80)	35.00–2.00 (2.03–2.00)	35.00–2.50 (2.54–2.50)	35.00–2.40 (2.44–2.40)
Completeness (%)[a]	86.1 (42.7)	97.6 (87.6)	99.9 (100.0)	99.6 (95.7)
R_{merge} (%)[a,b]	5.0 (60.0)	10.7 (47.8)	7.8 (64.0)	9.9 (79.3)
$I/\sigma I$[a]	37.2 (1.5)	28.4 (1.9)	34.9 (2.9)	50.0 (1.9)
Multiplicity[a]	6.8 (3.7)	5.9 (2.9)	15.8 (11.4)	22.0 (7.5)
Refinement				
Resolution (Å)	1.80	2.00	2.50	2.40
No. reflections; working/test	51829/2590	42682/2143	25616/1304	28612/1452
R_{work} (%)[c]	23.2	20.9	19.7	21.0
R_{free} (%)[d]	28.2	26.3	24.4	29.5
No. of protein atoms	5174	5184	5162	5144
No. of ligand atoms	2	3	2	2
No. of solvent sites	141	229	100	26
Average B factor (Å²)				
Protein	49.0	39.7	54.0	73.5
Zn (II)	36.9	31.3	55.2	64.8
Mg (II)	N/A	60.4	N/A	N/A
Solvent	40.8	38.7	42.5	59.1
Ramachandran statistics[e]				
Preferred (%)	93.01	94.07	93.76	91.32
Allowed (%)	4.56	4.10	4.11	5.18
Root mean square deviation				
Bond lengths (Å)	0.009	0.008	0.010	0.009
Bond angles (°)	1.249	1.149	1.175	1.236
PDB entry	4IG2	4IFK	4IFO	4IFR

[a] The values in parentheses are for the highest resolution shell.

[b] $R_{merge} = \Sigma_i |I_{hkl,i} - \langle I_{hkl} \rangle| / \Sigma_{hkl} \Sigma_i I_{hkl,i}$, where $I_{hkl,i}$ is the observed intensity, and $\langle I_{hkl} \rangle$ is the average intensity of multiple measurements.

[c] $R_{work} = \Sigma ||F_o| - |F_c|| / \Sigma |F_o|$, where $|F_o|$ is the observed structure factor amplitude, and $|F_c|$ is the calculated structure factor amplitude.

[d] R_{free} is the R factor based on 5% of the data excluded from refinement.

[e] Based on values attained from refinement validation options in COOT.

that the two conserved arginine residues that are being studied are proposed to bind the substrate, ACMS, which is unstable, so no binding constant can be easily measured. We have crafted a series of biochemical tests to show that *P. fluorescens* ACMSD must function as a dimer, and the two conserved arginine residues, including one intruded into the catalytic center from a neighboring subunit, are required for substrate binding in catalysis.

The molecular mechanism by which the catalytic activity is rescued through hybridization is illustrated in Fig. 4. During dimer-monomer equilibrium, three kinds of dimers form in solution when the two inactive homodimers of R51A and R239A are mixed: R51A homodimer, R239A homodimer, and R51A-R239A half-active heterodimer, in which one of the monomers has both Arg-51 and Arg-239 to constitute a complete active site identical to that of the native enzyme. If it is assumed that all homodimers are completely dissociated and rearranged, the percentage of formation of R51A homodimer and R239A homodimer will be both 25%. Consequently, the remaining 50% will be the half-active heterodimer. As a result, the maximum activity that can be rescued theoretically will be 25% of the wild-type ACMSD, assuming there is no cooperative interaction and that each of the dimers has the same association constant. By comparing the k_{cat} values of the equilibrated mixed mutant ACMSD with WT ACMSD, 9.2% of the theoretical maximum activity is recovered. The inability to recover more activity can likely be attributed to unequal equilibrium constants for each of the species (inactive homodimer forma-

tion may be thermodynamically preferred to half-active heterodimer formation), or some protein dynamics and cooperativity may have been lost because of the mutations of important active site residues.

To our knowledge, this x-ray crystallographic study provides the first unambiguous experimental evidence for the formation of hybridized active heterodimer by mixing of two inactive homodimers. These structures allow for a molecular level understanding of the correlation of enzymatic activity with the protein quaternary structure and the mechanism of activity rescue from two completely inactive mutants. Together with our previous work, we now can describe the functionally active assembly of the enzyme and the role of the two arginines in a more definitive manner as discussed below.

The homodimer structures contain a ~2,500 Å² dimer interface area. Prior to this work, the question of whether dimerization is an artificial aggregation or required for enzyme activity was not known. We showed here two major bands corresponding to monomer and dimer on the polyacrylamide gel, indicating the existence of both dimer and monomer forms in aqueous solution. Enzyme specific activities were measured under identical assay conditions using protein at different stock concentrations. The finding, *i.e.*, increasing specific activity with increasing protein stock concentrations, indicates that ACMSD is active when in the dimeric form and loses activity as it dissociates to the monomeric form.
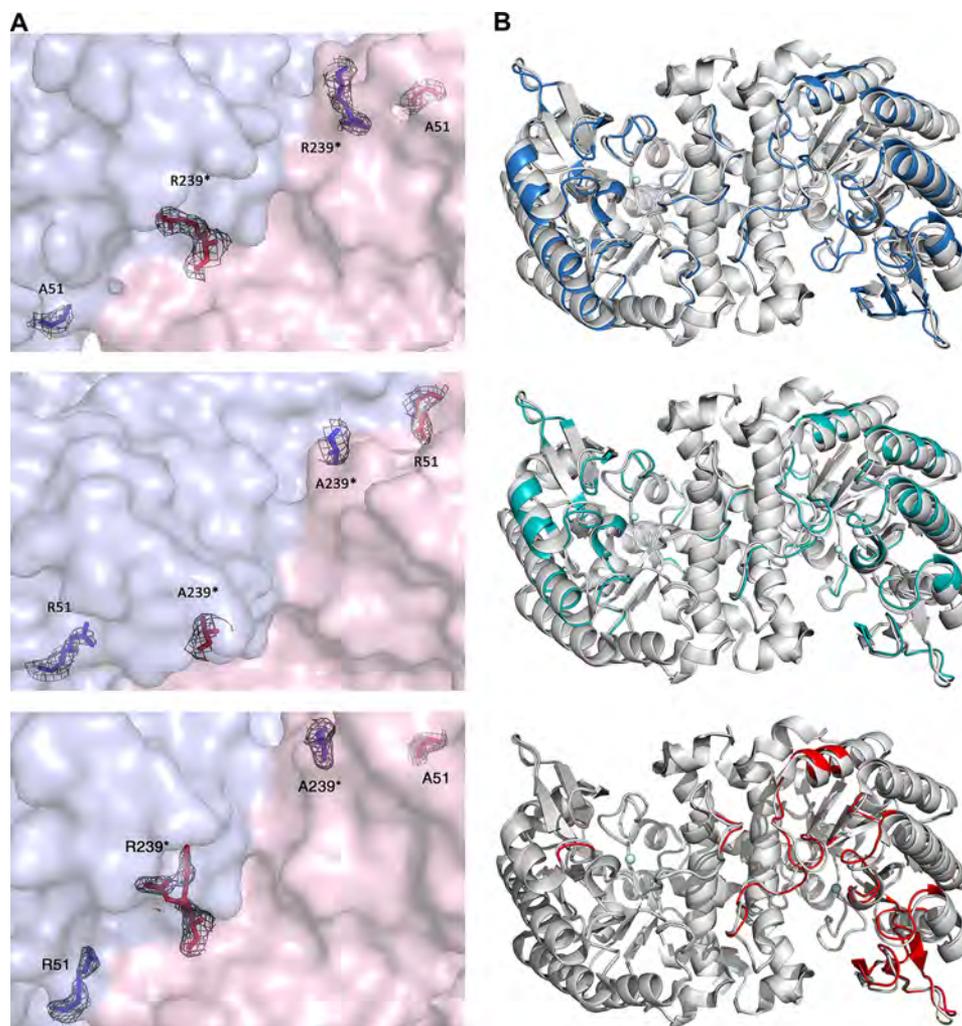
FIGURE 5. *A*, electron density of positions 51 and 239 in the R51A homodimer (*top panel*), R239A homodimer (*middle panel*), and R51A-R239A heterodimer (*bottom panel*). *B*, superimposed overall structures of WT Zn-ACMSD (Protein Data Bank code 2HBV) with Zn-R51A (Protein Data Bank code 4IFO) (*top panel*) and Zn-R239A (Protein Data Bank code 4IFR) (*middle panel*) and heterodimer hybrid (Protein Data Bank code 4IFK) (*bottom panel*). The well aligned structural components are shown in *gray*, whereas structural changes for R51A and R239A are highlighted in *blue* and *cyan*, respectively. Metal ions are represented by *spheres*. The graphs were produced using PyMOL. The $2F_o - F_c$ electron densities are contoured at 1.0 σ.

Dimer formation as a mechanism for enzyme activation is common in nature. Cytochrome *c* peroxidases (34), cell death protease caspases (35, 36), diaminopimelate epimerase (37), and histidine kinase CheA (38) are just a few examples similar to ACMSD. The reason behind this dimerization-induced activation is usually the generation or extension of binding faces at the dimer interface (39). Hence, protein activation is triggered by an increase in the local protein concentration. As calculated by the dependence of specific activity on stock enzyme concentration, the dissociation constant of ACMSD is 0.3 μM. This is within the K_d range for "weak" transient complexes that show a dynamic mixture of both monomer and dimer states *in vivo*, which could be tuned by physiological environmental factors such as pH and local protein or ligand concentrations (40).

The mutagenesis and reaction rescue experiments described in this study show that both Arg-51 and Arg-239 are required for enzyme activity. However, their role in catalysis was unknown because of the silent nature of their activity in all the point mutants, including the conservative Lys mutants, until the identification of an effective competitive inhibitor of the enzyme, PDC. By using this competitive inhibitor, the problems that arise from use of an unstable substrate can be mitigated. The inability of PDC to bind to the arginine mutants is demonstrated by the filtration experiment. With proper positive and negative controls, the designed experiment provides a straightforward and reliable conclusion. Hence, we propose that both arginine residues Arg-51 and Arg-239* are involved in substrate binding during catalysis (Fig. 7). It is noteworthy that this scenario resembles a well documented example in a high affinity nitrate transporter where two perfectly conserved arginine residues are required for substrate binding (41). Likewise, arginines play crucial roles in the active sites and subunit interfaces of the ATPase domains of AAA and AAA$^+$ proteins (for a recent review, see Ref. 42).

Heterodimer-induced activity restoration has also been previously observed, although not structurally characterized, in histidine protein kinase CheA, a protein essential for bacterial chemotaxis stimulus-response coupling by phosphorylating another two chemotaxis proteins: CheY and CheB (43). CheA must be autophosphorylated at its own His-48 residue before
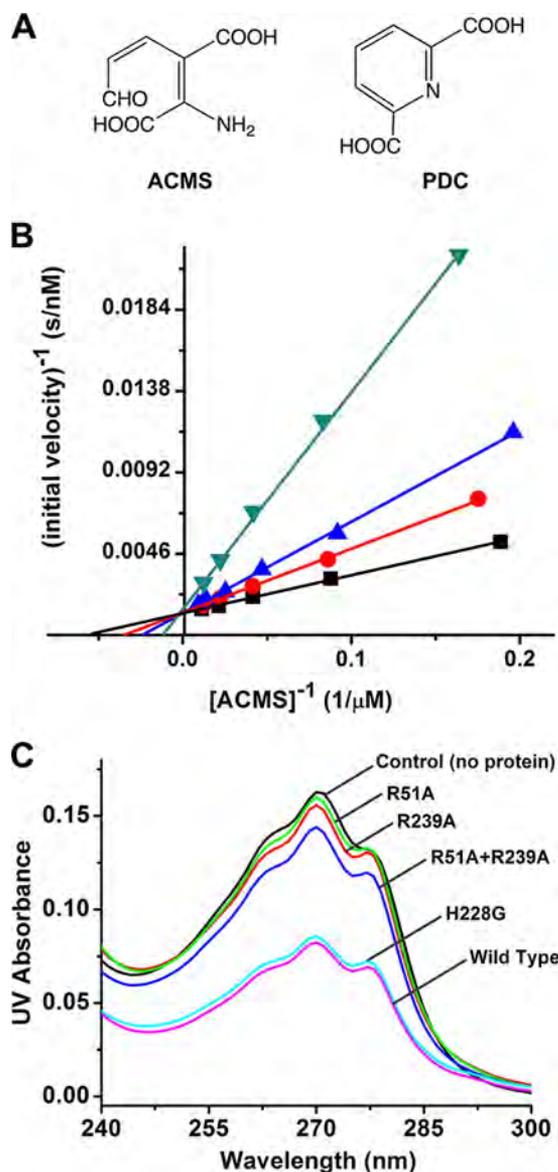
FIGURE 6. *A*, chemical structure of ACMS and PDC. *B*, competitive inhibition of wild-type ACMSD by 0, 20, 40, and 80 μM of PDC as the *black*, *red*, *blue*, and *green traces*, respectively. *C*, PDC in flow through after centrifuge-based filtration detected by UV-visible spectroscopy.

FIGURE 7. **Proposed role of Arg-51 and Arg-239* in ACMS decarboxylation mechanism.** The *asterisk* designates a residue contributed from a neighboring subunit. Currently, it is unknown in which way the substrate is oriented in the active site. Therefore, the presented mechanism represents one possible orientation, not necessarily the correct orientation.

this phosphoryl group can be transferred to CheY and CheB (44, 45). *E. coli* expresses two kinds of CheA proteins: the full-length CheAL and the N-terminally truncated CheAS, which lacks His-48, the site of autophosphorylation (44). However, in the presence of both CheAS and kinase defective CheAL mutant, CheA470GK, the mutant can still be phosphorylated. Thus, the autophosphorylation accomplished within the CheAS-CheA470GK heterodimer is suggested even in the absence of structural proof as shown in the present study (38).

The results described in this work helped us further refine our working model for the ACMSD catalytic cycle. Previously, the roles of His-228 and the metal-bound water were proposed and demonstrated (22). The two catalytically essential arginine residues Arg-51 and Arg-239* are now added to the model (Fig. 7). They are proposed to work as a team to recognize the substrate and stabilize both the substrate and possibly catalytic intermediates. Because the two residues at each metal center
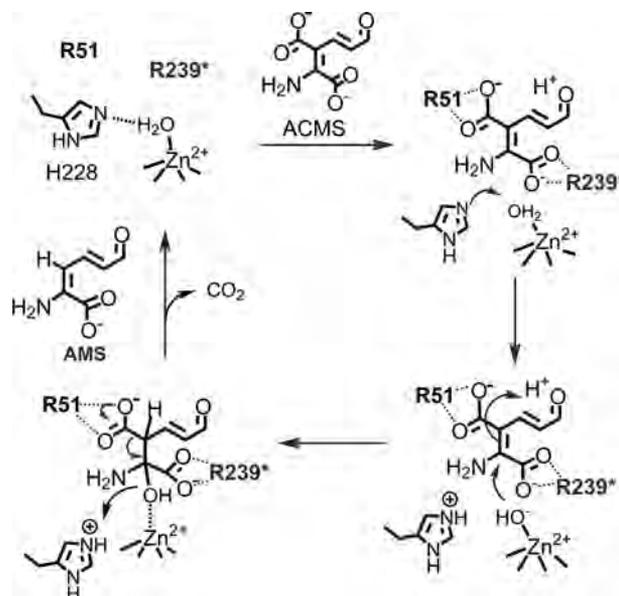
belong to two different subunits, the requirement of protein dimerization for enzyme activity becomes evident.

Among cellular metabolic proteins, monomers are a small fraction compared with multimeric proteins. Homodimers and homotetramers are two major forms of oligomerized proteins (39). Compared with monomeric proteins, oligomerized proteins have some apparent advantages. First, oligomerization enables higher order protein regulation, such as allosteric and concentration sensing regulations. Second, protein oligomerization can help to increase protein stability and the flexibility of activity by subunit cooperation. Lastly, homo-oligomers are more economic because they allow for a smaller genome while still building large proteins. Hence, the oligomerization of ACMSD may function as a mechanism of protein concentration sensing and enzyme activity adjustment *in vivo*.

REFERENCES

1. Donald, J. E., Kulp, D. W., and DeGrado, W. F. (2011) Salt bridges. Geometrically specific, designable interactions. *Proteins* **79,** 898–915
2. Prell, J. S., O'Brien, J. T., Steill, J. D., Oomens, J., and Williams, E. R. (2009) Structures of protonated dipeptides. The role of arginine in stabilizing salt bridges. *J. Am. Chem. Soc.* **131,** 11442–11449
3. Ghosh, M., and Datta, A. K. (1994) Probing the function(s) of active-site arginine residue in leishmania-donovani adenosine kinase. *Biochem. J.* **298,** 295–301
4. Reczkowski, R. S., Taylor, J. C., and Markham, G. D. (1998) The active-site arginine of *S*-adenosylmethionine synthetase orients the reaction intermediate. *Biochemistry* **37,** 13499–13506
5. Chaidaroglou, A., Brezinski, D. J., Middleton, S. A., and Kantrowitz, E. R. (1988) Function of arginine-166 in the active site of *Escherichia coli* alkaline phosphatase. *Biochemistry* **27,** 8338–8343
6. Blachnio, K., and Przykorska, A. (2005) Specific arginine mediated RNA

recognition. *Postepy. Biochem.* **51,** 339–344

7. Charnock, S. J., Brown, I. E., Turkenburg, J. P., Black, G. W., and Davies, G. J. (2002) Convergent evolution sheds light on the anti-β-elimination mechanism common to family 1 and 10 polysaccharide lyases. *Proc. Natl. Acad. Sci. U.S.A.* **99,** 12067–12072

8. GuillénSchlippe, Y. V., and Hedstrom, L. (2005) Is Arg418 the catalytic base required for the hydrolysis step of the IMP dehydrogenase reaction? *Biochemistry* **44,** 11700–11707

9. Doherty, M. K., Pealing, S. L., Miles, C. S., Moysey, R., Taylor, P., Walkinshaw, M. D., Reid, G. A., and Chapman, S. K. (2000) Identification of the active site acid/base catalyst in a bacterial fumarate reductase. A kinetic and crystallographic study. *Biochemistry* **39,** 10695–10701

10. Li, T., Iwaki, H., Fu, R., Hasegawa, Y., Zhang, H., and Liu, A. (2006) α-Amino-β-carboxymuconic-ε-semialdehyde decarboxylase (ACMSD) is a new member of the amidohydrolase superfamily. *Biochemistry* **45,** 6628–6634

11. Li, T., Walker, A. L., Iwaki, H., Hasegawa, Y., and Liu, A. (2005) Kinetic and spectroscopic characterization of ACMSD from *Pseudomonas fluorescens* reveals a pentacoordinate mononuclear metallocofactor. *J. Am. Chem. Soc.* **127,** 12282–12290

12. Stone, T. W., and Darlington, L. G. (2002) Endogenous kynurenines as targets for drug discovery and development. *Nat. Rev. Drug Discov.* **1,** 609–620

13. Schwarcz, R. (2004) The kynurenine pathway of tryptophan degradation as a drug target. *Curr. Opin. Pharmacol.* **4,** 12–17

14. Mehler, A. H., Yano, K., and May, E. L. (1964) Nicotinic acid biosynthesis. Control by an enzyme that competes with a spontaneous reaction. *Science* **145,** 817–819

15. Colabroy, K. L., and Begley, T. P. (2005) The pyridine ring of NAD is formed by a nonenzymatic pericyclic reaction. *J. Am. Chem. Soc.* **127,** 840–841

16. Guillemin, G. J., Williams, K. R., Smith, D. G., Smythe, G. A., Croitoru-Lamoury, J., and Brew, B. J. (2003) Developments in tryptophan and serotonin metabolism. Quinolinic acid in the pathogenesis of Alzheimer's disease. *Adv. Exp. Med. Biol.* **527,** 167–176

17. Guidetti, P., and Schwarcz, R. (2003) 3-Hydroxykynurenine and quinolinate. pathogenic synergism in early grade Huntington's disease? *Adv. Exp. Med. Biol.* **527,** 137–145

18. Reinhard, J. F., Jr. (2004) Pharmacological manipulation of brain kynurenine metabolism. *Ann. N.Y. Acad. Sci.* **1035,** 335–349

19. Martynowski, D., Eyobo, Y., Li, T., Yang, K., Liu, A., and Zhang, H. (2006) Crystal structure of α-amino-β-carboxymuconic-ε-semialdehyde decarboxylase (ACMSD). Insight into the active site and catalytic mechanism of a novel decarboxylation reaction. *Biochemistry* **45,** 10412–10421

20. Garavaglia, S., Perozzi, S., Galeazzi, L., Raffaelli, N., and Rizzi, M. (2009) The crystal structure of human α-amino-β-carboxymuconate-ε-semialdehyde decarboxylase in complex with 1,3-dihydroxyacetonephosphate suggests a regulatory link between NAD synthesis and glycolysis. *FEBS J.* **276,** 6615–6623

21. Pucci, L., Perozzi, S., Cimadamore, F., Orsomando, G., and Raffaelli, N. (2007) Tissue expression and biochemical characterization of human 2-amino 3-carboxymuconate 6-semialdehyde decarboxylase, a key enzyme in tryptophan catabolism. *FEBS J.* **274,** 827–840

22. Huo, L., Fielding, A. J., Chen, Y., Li, T., Iwaki, H., Hosler, J. P., Chen, L., Hasegawa, Y., Que, L., Jr., and Liu, A. (2012) Evidence for a dual role of an active site histidine in α-amino-β-carboxymuconic-ε-semialdehyde decarboxylase. *Biochemistry* **51,** 5811–5821

23. Horton, R. M. (1995) PCR-mediated recombination and mutagenesis. SOEing together tailor-made genes. *Mol. Biotechnol.* **3,** 93–99

24. Li, T., Ma, J. K., Hosler, J. P., Davidson, V. L., and Liu, A. (2007) Detection of transient intermediates in the metal-dependent non-oxidative decarboxylation catalyzed by α-amino-β-carboxymuconic-ε-semialdehyde decarboxylase. *J. Am. Chem. Soc.* **129,** 9278–9279

25. Koontz, W. A., and Shiman, R. (1976) Beef kidney 3-hydroxyanthranilic acid oxygenase. Purification, characterization, and analysis of the assay. *J. Biol. Chem.* **251,** 368–377

26. Otwinowski, Z., and Minor, W. (1997) Processing of x-ray diffraction data collected in oscillation mode. *Method Enzymol.* **276,** 307–326

27. Vagin, A., and Teplyakov, A. (2010) Molecular replacement with MOLREP. *Acta Crystallogr. D Biol. Crystallogr.* **66,** 22–25

28. Collaborative Computational Project, Number 4 (1994) The Ccp4 suite. Programs for protein crystallography. *Acta Crystallogr. D Biol. Crystallogr.* **50,** 760–763

29. Adams, P. D., Afonine, P. V., Bunkóczi, G., Chen, V. B., Davis, I. W., Echols, N., Headd, J. J., Hung, L. W., Kapral, G. J., Grosse-Kunstleve, R. W., McCoy, A. J., Moriarty, N. W., Oeffner, R., Read, R. J., Richardson, D. C., Richardson, J. S., Terwilliger, T. C., and Zwart, P. H. (2010) PHENIX. A comprehensive Python-based system for macromolecular structure solution. *Acta Crystallogr. D Biol. Crystallogr.* **66,** 213–221

30. Emsley, P., and Cowtan, K. (2004) Coot. Model-building tools for molecular graphics. *Acta Crystallogr. D Biol. Crystallogr.* **60,** 2126–2132

31. Krissinel, E., and Henrick, K. (2007) Inference of macromolecular assemblies from crystalline state. *J. Mol. Biol.* **372,** 774–797

32. Fukuwatari, T., Ohsaki, S., Fukuoka, S., Sasaki, R., and Shibata, K. (2004) Phthalate esters enhance quinolinate production by inhibiting α-amino-β-carboxymuconate-ε-semialdehyde decarboxylase (ACMSD), a key enzyme of the tryptophan pathway. *Toxicol. Sci.* **81,** 302–308

33. Fukuwatari, T., Ohsaki, S., Suzuki, Y., Fukuoka, S., Sasaki, R., and Shibata, K. (2003) The effects of phthalate esters on the tryptophan-niacin metabolism. *Adv. Exp. Med. Biol.* **527,** 659–664

34. Ellis, K. E., Frato, K. E., and Elliott, S. J. (2012) Impact of quaternary structure upon bacterial cytochrome *c* peroxidases. Does homodimerization matter? *Biochemistry* **51,** 10008–10016

35. Renatus, M., Stennicke, H. R., Scott, F. L., Liddington, R. C., and Salvesen, G. S. (2001) Dimer formation drives the activation of the cell death protease caspase 9. *Proc. Natl. Acad. Sci. U.S.A.* **98,** 14250–14255

36. Datta, D., McClendon, C. L., Jacobson, M. P., and Wells, J. A. (2013) Substrate and inhibitor-induced dimerization and cooperativity in caspase-1 but not caspase-3. *J. Biol. Chem.* **288,** 9971–9981

37. Hor, L., Dobson, R. C., Downton, M. T., Wagner, J., Hutton, C. A., and Perugini, M. A. (2013) Dimerization of bacterial diaminopimelate epimerase is essential for catalysis. *J. Biol. Chem.* **288,** 9238–9248

38. Swanson, R. V., Bourret, R. B., and Simon, M. I. (1993) Intermolecular complementation of the kinase activity of CheA. *Mol. Microbiol.* **8,** 435–441

39. Marianayagam, N. J., Sunde, M., and Matthews, J. M. (2004) The power of two. Protein dimerization in biology. *Trends Biochem. Sci.* **29,** 618–625

40. Nooren, I. M., and Thornton, J. M. (2003) Structural characterisation and functional significance of transient protein-protein interactions. *J. Mol. Biol.* **325,** 991–1018

41. Unkles, S. E., Rouch, D. A., Wang, Y., Siddiqi, M. Y., Glass, A. D., and Kinghorn, J. R. (2004) Two perfectly conserved arginine residues are required for substrate binding in a high-affinity nitrate transporter. *Proc. Natl. Acad. Sci. U.S.A.* **101,** 17549–17554

42. Ogura, T., Whiteheart, S. W., and Wilkinson, A. J. (2004) Conserved arginine residues implicated in ATP hydrolysis, nucleotide-sensing, and inter-subunit interactions in AAA and AAA$^+$ ATPases. *J. Struct. Biol.* **146,** 106–112

43. Parkinson, J. S., and Kofoid, E. C. (1992) Communication modules in bacterial signaling proteins. *Annu. Rev. Genet.* **26,** 71–112

44. Hess, J. F., Bourret, R. B., and Simon, M. I. (1988) Histidine phosphorylation and phosphoryl group transfer in bacterial chemotaxis. *Nature* **336,** 139–143

45. Hess, J. F., Oosawa, K., Matsumura, P., and Simon, M. I. (1987) Protein phosphorylation is involved in bacterial chemotaxis. *Proc. Natl. Acad. Sci. U.S.A.* **84,** 7609–7613